Sustainable Marine Structures
https://journals.nasspublishing.com/index.php/sms

ARTICLE

Numerical Prediction of the Seismic Behavior of Offshore Skirted Foundations Accounting for the Separate Influences of Soil and Superstructure Inertia

Alaoua Bouaicha [1*] **, *Nassima Zatar*** [2]

[1] *Scientific and Technical Research Center on Arid Regions (CRSTRA), Campus of Mohamed Khider University, BP 1682 RP, Biskra 07000, Algeria*

[2] *Civil Engineering Department, Faculty of Technology, University Mostafa Benboulaid, Batna 05078, Algeria*

ABSTRACT

The seismic behavior of skirted foundations plays a crucial role in the stability of marine and coastal structures subjected to earthquakes. This study provides an in-depth examination of the seismic bearing response of skirted foundations subjected to eccentric vertical loading, assessed through a Finite Element Limit Analysis (FELA) framework. The objective is to separately characterize the inertial contributions of the soil mass and the superstructure as functions of the horizontal seismic coefficient k_h, the relative skirt depth D/B, and the eccentricity ratio e/B. Unlike previous studies, which generally consider inertial effects in a simplified or combined manner, this work introduces a systematic and explicit separation of soil and superstructure inertia contributions for skirted foundations within a unified numerical framework, particularly under eccentric loading conditions. This approach enables a clearer distinction between local soil failure mechanisms and global structural effects, thereby improving the understanding of the seismic response of skirted foundations. The findings reveal the decisive role of skirt embedment depth, which enhances stability and delays failure, whereas increasing k_h and e/B significantly reduces the bearing capacity. The resulting three-dimensional surfaces offer a clear visualization of the combined influence of these parameters, revealing critical operational zones and stability domains of skirted foundations under seismic load-

*CORRESPONDING AUTHOR:
Alaoua Bouaicha, Scientific and Technical Research Center on Arid Regions (CRSTRA), Campus of Mohamed Khider University, BP 1682 RP, Biskra 07000, Algeria; Email: alaoua.bouaicha@univ-biskra.dz

ARTICLE INFO
Received: 19 March 2026 | Revised: 25 May 2026 | Accepted: 1 June 2026 | Published Online: 5 June 2026
DOI: https://doi.org/10.36956/sms.v8i2.3300

CITATION
Bouaicha, A., Zatar, N., 2026. Numerical Prediction of the Seismic Behavior of Offshore Skirted Foundations Accounting for the Separate Influences of Soil and Superstructure Inertia. Sustainable Marine Structures. 8(2): 206–224. DOI: https://doi.org/10.36956/sms.v8i2.3300

ing. Two new generalized analytical equations were developed for the correction factors associated under inertial effects, showing excellent agreement with the FELA results. These formulations, combined with the developed 3D surfaces, provide practical and reliable tools for optimized seismic design of skirted foundations under seismic conditions.

Keywords: Eccentric Loading; FELA; Skirted Foundations; Seismic Bearing Capacity; Soil and Superstructure Inertia

1. Introduction

The reliable estimation of the bearing capacity of shallow foundations remains a key challenge for geotechnical applications, particularly in regions exposed to seismic loading. This issue is of particular importance in marine and coastal environments, where foundations are subjected to complex loading conditions induced by waves, currents, and seismic actions, as encountered in offshore platforms, wind turbines, and port infrastructures. Since the pioneering work [1], significant advances have been made through analytical, experimental, and numerical approaches, refining the understanding of failure mechanisms and influencing parameters [2–4].

Within this evolution, skirted foundations have emerged as an efficient design solution, mainly due to the confinement of a rigid soil plug beneath the footing, which substantially improves the bearing capacity and reduces settlements [5–7]. Their efficiency is particularly remarkable under horizontal or seismic loading, as confirmed by numerous numerical and experimental studies carried out in offshore and coastal environments [8–12].

Regarding seismic bearing capacity, several pseudo-static frameworks have been developed for shallow foundations and have progressively served as the basis for the analysis of skirted foundations. The works [13, 14] explicitly introduced horizontal accelerations into failure mechanisms. These approaches were further refined [15, 16] and more recently extended [17] through numerical analyses incorporating foundation geometry, load direction, and inertial effects. These contributions have enhanced the understanding of the seismic response of shallow and partially embedded foundations.

For skirted foundations, several recent studies have strengthened theoretical and numerical frameworks, particularly through limit analysis [18, 19] and slip-line theory [20]. However, most of these investigations consider separately the two major effects: soil inertia (body forces) and superstructure inertia (base shear and moment inducing an effective eccentricity). The combined quantification of these two contributions, interacting with the skirt geometry, remains only partially explored.

Recent studies have further advanced the understanding of the seismic behavior of skirted foundations. For instance, shaking table tests and three-dimensional numerical analyses have highlighted the significant role of skirt confinement in enhancing soil stability and reducing liquefaction potential beneath offshore foundations [21]. In parallel, hybrid approaches combining Finite Element Limit Analysis (FELA) with machine learning techniques have been developed to predict seismic bearing capacity under complex conditions, such as slopes and inclined loading, demonstrating high predictive accuracy and efficiency [22, 23]. Other recent investigations have focused on the influence of soil type and geometry, showing that skirted foundations significantly improve bearing capacity and modify failure mechanisms under seismic loading, particularly in cohesive or cohesive-frictional soils and sloping ground conditions [24, 25]. Despite these advances, most studies primarily address specific configurations or loading conditions, and a comprehensive framework that clearly distinguishes and quantifies the respective contributions of soil inertia and superstructure inertia remains limited.

The present study aims to characterize the seismic bearing capacity of skirted foundations subjected to eccentric vertical loading, taking into account both soil and superstructure inertia. The investigation is carried out for a homogeneous frictional soil (φ = 30°), sys-

tematically exploring the combined effects of the horizontal seismic coefficient k_h, the eccentricity ratio e/B, and the relative skirt depth D/B. The methodology is based on a series of FELA simulations designed to isolate and quantify these inertial contributions within a unified numerical framework. While previous studies have investigated seismic bearing capacity or inertial effects in skirted or shallow foundations, they generally consider soil inertia and superstructure inertia either separately or through simplified combined approaches. In contrast, the present study provides a systematic and explicit distinction between these two contributions, particularly under eccentric loading conditions, allowing a clearer identification of their respective roles in the failure mechanism and bearing capacity degradation. The results include the evolution of the bearing capacity under combined inertial effects, the development of three-dimensional design charts, and the derivation of generalized analytical equations for correction factors associated with soil and superstructure inertia. These outcomes provide both new insights into the seismic behavior of skirted foundations and practical tools for engineering design, facilitating a more accurate assessment of their performance under complex seismic loading conditions.

2. Problem Statement

The present study focuses on the seismic bearing capacity of skirted foundations consisting of a rigid strip footing of width B, equipped with vertical skirts of depth D, characterized by the relative embedment ratio D/B. These foundations rest on the surface of a purely frictional soil (c = 0, q = 0) and are subjected to a vertically eccentric load defined by the ratio e/B.

The seismic loading is modeled through a pseudo-static approach considering only the horizontal acceleration (k_v = 0), in order to isolate the effect of lateral inertia on the failure mechanism. This simplified approach is commonly adopted in seismic bearing capacity analyses and provides an efficient framework for preliminary evaluation and parametric investigations of foundation stability under earthquake loading. However, it does not account for transient dynamic effects, wave propagation, cyclic loading, or frequency-dependent soil response, and may therefore become less reliable under strong seismic events, liquefaction conditions, or highly nonlinear dynamic soil behavior. Nevertheless, within the investigated parameter range, the pseudo-static method provides a consistent and practical approximation for evaluating the influence of seismic inertia on the bearing capacity of skirted foundations.

In addition, neglecting the vertical seismic acceleration may influence the predicted bearing capacity, since an upward vertical acceleration tends to reduce the normal stresses beneath the foundation and consequently decrease the bearing resistance, whereas a downward acceleration may partially increase the confinement effect[17]. Nevertheless, the assumption $k_v = 0$ remains widely adopted in pseudo-static analyses and provides a simplified and consistent framework for investigating the influence of horizontal seismic inertia on the behavior of skirted foundations.

In the absence of cohesion and surcharge, the ultimate bearing capacity of the soil can be expressed in its generalized form as:

$$V_{ultE} = \frac{1}{2}\gamma B N_{\gamma E} \tag{1}$$

where $N_{\gamma E}$ denotes the seismic factor associated with the unit weight γ, which depends on the horizontal seismic coefficient k_h, the relative skirt depth D/B, and the eccentricity ratio e/B.

The eccentricity of the applied load (e/B) is explicitly accounted for in all analyzed cases. It modifies the stress distribution beneath the foundation, promotes an asymmetric extension of the plastic zones beneath the skirts, and affects the overall kinematics of failure. This approach enables a realistic representation of actual loading conditions, where eccentricity arises from the combined effects of the transmitted superstructure loads, the orientation of external actions, and the geometric characteristics of the foundation—thus moving beyond the simplifying assumption of a centrally applied load.

To isolate the respective inertial contributions, two independent loading cases are analyzed (**Figure 1**):

- Case 1—Soil inertia effect: A uniform horizontal body force $k_h\gamma$ is applied to the soil mass (k_v = 0), while the vertical load remains eccentric. This con-

figuration allows the determination of the factor $N^{s}_{\gamma E}$, representing the portion of seismic resistance attributable to the soil behavior involved in the failure mechanism (**Figure 1a**).

- Case 2—Superstructure inertia effect: No body force is applied to the soil; the seismic action is introduced as equivalent base loads, namely a horizontal shear H and a moment M, corresponding to an effective eccentricity $e = M/V$. This configuration yields the factor $N^{ss}_{\gamma E}$, which expresses the specific contribution of the superstructure inertia to the reduction of the bearing capacity (**Figure 1b**).

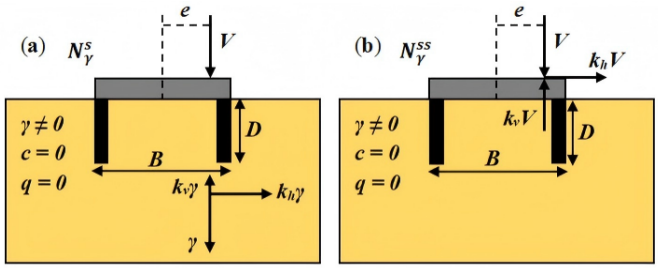

Figure 1. Schematic illustration of the adopted seismic loading conditions: (**a**) soil inertia effect, (**b**) superstructure inertia effect.

The comparison and combination of these two effects are made with reference to a unique baseline: the static bearing capacity factor N_γ of a surface foundation without skirts ($D/B = 0$) and subjected to a centered load ($k_h = 0$, $e/B = 0$). Two correction coefficients, functions of D/B, k_h, and e/B, are introduced and numerically calibrated as follows:

$$e^{s}_{\gamma E} = \frac{N^{s}_{\gamma E}}{N_\gamma}, \qquad e^{ss}_{\gamma E} = \frac{N^{ss}_{\gamma E}}{N_\gamma} \tag{2}$$

The soil is modeled as a homogeneous, purely frictional medium ($c = 0$, $\varphi = 30°$), obeying the Mohr–Coulomb yield criterion with perfect plasticity. The foundation is assumed rigid and equipped with vertical skirts of depth D. A fully rough interface condition is adopted ($\delta = \varphi$ or $\delta/\varphi = 1$), reflecting a strongly interlocking soil–structure interaction. This assumption—commonly accepted in the literature—defines the upper bound of mobilized bearing capacity for skirted foundations and establishes the framework for developing reduction curves, design charts, and generalized dimensioning equations [17].

Recent studies on geomaterial failure under complex stress states have also highlighted the importance of stress orientation and anisotropy on strength evolution and failure mechanisms. For instance, true triaxial compression tests performed on weakly anisotropic sandstone demonstrated that the magnitudes and directions of principal stresses significantly influence the failure pattern, strength anisotropy, and shear localization processes, particularly under coupled stress conditions. The study further showed that the interaction between structural anisotropy and stress-induced anisotropy plays a key role in the development of failure mechanisms and strength envelopes under complex loading paths [26].

2.1. Numerical Modeling Procedure

The numerical simulations were conducted using the OptumG2 software [27], adopting the Finite Element Limit Analysis (FELA) approach to evaluate the seismic bearing capacity of a skirted foundation subjected to combined loading involving both eccentricity and the pseudo-static effect of earthquake forces.

In this framework, the lower bound (LB) and upper bound (UB) limit analysis formulations are implemented through two complementary formulations. The LB formulation is based on searching for equilibrium-admissible stress fields that simultaneously satisfy the equilibrium equations and the yield criterion, whereas the UB formulation is established through the construction of kinematically admissible velocity fields consistent with the flow rule and internal energy dissipation [28]. The distinction between these two approaches allows a rigorous bracketing of the collapse load and ensures the numerical reliability of the obtained results.

Due to the presence of an eccentric load and horizontal pseudo-static body forces, the model was built without symmetry and evaluated within a two-

dimensional plane strain framework. The bottom boundary of the computational domain was fully restrained against both horizontal and vertical displacements, while the lateral faces are restrained horizontally and free vertically, and the ground surface is left free (**Figure 2**). To eliminate any artificial boundary influence on the failure mechanism, a sufficiently large computational domain was adopted, with a width equal to 20B and a total depth of 5B. These proportions—established through preliminary tests—are consistent with commonly adopted guidelines for finite element modeling of shallow foundations and ensure the natural development of plastic zones.

The adaptive meshing capability was utilized to concentrate refinement in areas of high shear dissipation [29–31]. Three successive automatic refinement cycles were applied: starting from an initial mesh of approximately 1,000 elements, the total number could reach up to 25,000 elements, depending on the configuration analyzed. This procedure stabilizes the LB/UB limits, improves the accuracy of the collapse load, and accurately captures the extent of plasticized zones and shear bands [4, 12].

The loading was applied using the probe loading method, which consists of progressively imposing a vertical load with a prescribed eccentricity (e/B), while introducing the seismic action as a uniform horizontal body force $k_h\gamma$ (with k_v = 0). This procedure enables the separate and combined examination of the effects of soil inertia (for k_h > 0 with an imposed eccentricity) and superstructure inertia (for k_h = 0 when the seismic action is introduced as equivalent base loads H and M, corresponding to an effective eccentricity $e = M/V$). For each parameter combination (D/B, k_h, e/B), the ultimate load is determined by bracketing the solution between the lower and upper bounds, and their mean value is then adopted to obtain a unique, stable, and representative estimate of the seismic bearing capacity of the skirted foundation [3, 4].

In addition, preliminary sensitivity analyses confirmed that further increases in the computational domain dimensions or additional mesh refinement produced only negligible variations in the ultimate load. Furthermore, the difference between the lower-bound (LB) and upper-bound (UB) solutions generally remained within approximately 3–5% over the entire investigated parameter range. Such a relatively small LB/UB gap indicates good numerical stability, satisfactory convergence behavior, and a reliable estimation of the collapse load within the adopted FELA framework.

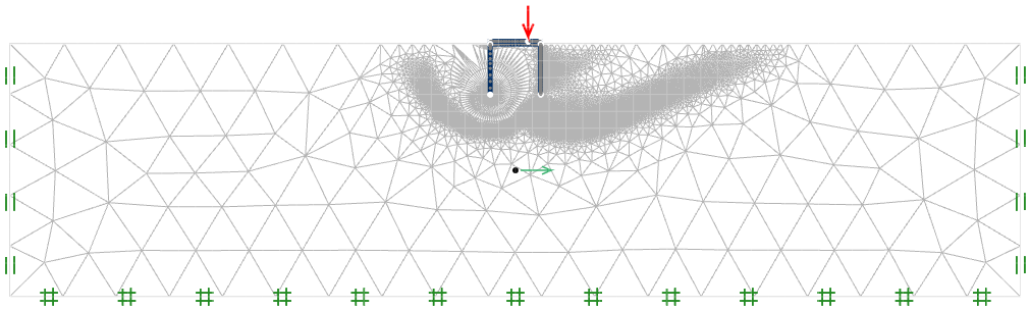

Figure 2. Failure mechanism and adaptive mesh distribution for φ = 30°, e/B = 0.25, D/B = 1 and k_h = 0.2.

2.2. Model Validation

Within the framework of the Finite Element Limit Analysis (FELA), each simulation provides a bracketing of the ultimate load between a lower bound (LB) and an upper bound (UB), whose relative difference serves as a direct indicator of numerical accuracy. For comparison and reference purposes, the arithmetic mean (Average) of these two bounds is adopted as a representative and stable estimate of the collapse load and the corresponding bearing capacity factors.

The first validation case concerns a skirted foundation on dry sand (c = 0, φ = 30°) subjected to a centered vertical load (e/B = 0) and analyzed under static conditions (k_h = 0). **Table 1** compares the results obtained using FELA (LB, UB, and Average) with three major references from the literature [18, 20, 32], involving upper-bound limit analysis with a multi-block failure mechanism, slip-line theory, and an upper-bound finite-element formulation for embedded footings. An overall excellent agreement is observed across the full range of embedment ratios.

Table 1. Comparative analysis of the bearing capacity factor N_γ under static conditions for skirted foundations.

φ (°)	D/B	Pal et al. [18]	Santhoshkumar and Ghosh [20]	Mohapatra and Kumar [32]	Present Study		
					LB	UB	Avg.
15	0.0	1.93	1.71	–	1.16	1.20	1.18
	0.6	7.3	6.32	–	7.04	7.21	7.13
	1.0	10.23	9.34	–	10.99	11.22	11.11
20	0.0	4.47	3.82	2.94	2.78	2.88	2.83
	0.6	13.85	12.36	13.86	13.38	13.80	13.59
	1.0	20.65	17.91	21.01	20.40	20.96	20.68
25	0.0	9.77	8.44	–	6.30	6.60	6.45
	0.6	25.9	23.74	–	25.09	25.95	25.52
	1.0	37.68	33.72	–	37.48	38.63	38.05
30	0.0	21.41	18.46	15.6	14.28	15.03	14.65
	0.6	49.6	46.31	49.78	48.23	50.12	49.17
	1.0	70.08	64.56	72.59	70.33	73.14	71.74

The results from the present study consistently fall between the slip-line theory solutions—generally more conservative—and the upper-bound estimates, which tend to be slightly higher. The LB and UB results closely bracket the average value, indicating low internal dispersion and confirming both the numerical robustness and the reliability of the model for skirted foundations under static conditions.

Figure 3 illustrates, for a soil with $\varphi = 30°$, $D/B = 0$, and $e/B = 0$, the variation of the seismic correction factor as a function of the horizontal seismic coefficient k_h, distinguishing **Figure 3a** the effect of soil inertia and **Figure 3b** the effect of superstructure inertia. In both cases, a clearly decreasing trend is observed, with an accentuated curvature as k_h increases, reflecting the progressive degradation of bearing capacity under seismic excitation. The results obtained in this study—expressed as the average between LB and UB—fall within the envelope of solutions available in the literature and are particularly close to those reported in the study by Cascone and Casablanca [16], while remaining between the higher estimates in the study by Paolucci and Pecker [15] and the more conservative predictions in the study by Conti [33]. This overall consistency, observed for both inertial effects, demonstrates the numerical stability of the FELA model and further strengthens the credibility of the predicted responses for skirted foundations under seismic conditions. **Figure 3c** presents the validation of the combined inertial effect by comparing the seismic correction factor obtained in the present study with the reference solution reported by Cascone and Casablanca [16]. A very good agreement is observed over the entire range of the horizontal seismic coefficient k_h, with both curves exhibiting the same nonlinear decreasing trend. As k_h increases, the seismic correction factor progressively decreases, reflecting the combined destabilizing influence of soil inertia and superstructure inertia on the bearing capacity. The close agreement between the present FELA results and the published reference confirms the ability of the adopted numerical framework to accurately reproduce the coupled seismic response under combined inertial loading. This validation also supports the relevance of separately analyzing soil and superstructure inertia in order to better understand their individual contributions before addressing fully coupled skirted foundation configurations.

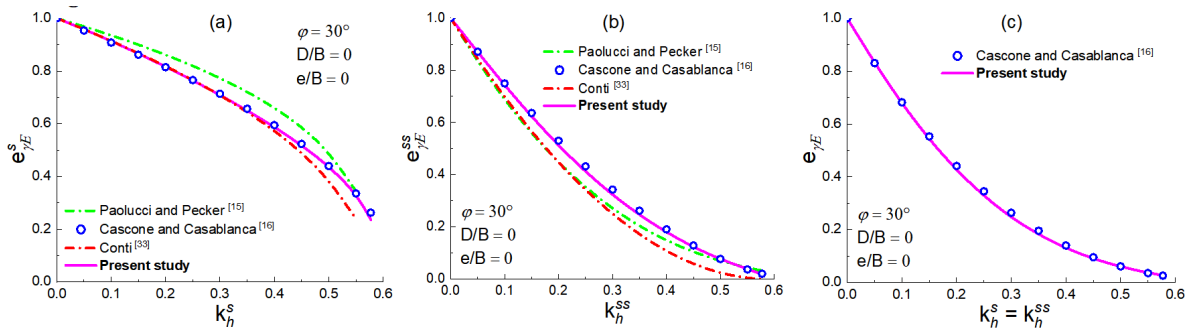

Figure 3. Comparison of the correction factor for $\varphi = 30°$, $D/B = 0$, and $e/B = 0$: (**a**) soil inertia effect, (**b**) superstructure inertia effect, (**c**) combined effect.

3. Results and Discussions

To systematically investigate the seismic bearing capacity of skirted foundations, a comprehensive parametric study was conducted by varying the main parameters of the problem. The soil was assumed to be purely frictional (φ = 30°), and the seismic action was modeled using a pseudo-static approach with k_v = 0. The horizontal seismic coefficient k_h was progressively increased up to the limiting value $k_{h,limit} = tan\varphi$, which is conventionally associated with the complete loss of mobilized shear resistance [16, 17]. The relative skirt embedment ratio D/B was explored for four representative values (D/B = 0.1, 0.25, 0.5, and 1), while the normalized eccentricity of the vertical load covered a wide range e/B = {0, 0.025, 0.05, 0.075, 0.1, 0.15, 0.25, 0.35, 0.45}. The base–skirt–soil interface was assumed to be perfectly rough (δ/φ = 1). All results are presented in terms of seismic factors and correction coefficients, enabling a clear distinction between the respective effects of soil inertia and superstructure inertia.

Figure 4 illustrates, for φ = 30°, the decay of the seismic factor $N^s_{\gamma E}$ as a function of k^s_h. The results reveal that the confinement provided by the skirts consistently elevates the curve and reduces its slope, whereas the load eccentricity lowers the initial level and increases the sensitivity of bearing capacity to seismic effects, particularly for shallow skirts. In the centered configuration (**Figure 4a**), a deep skirt (D/B = 1) exhibits only about a 23% reduction between k^s_h = 0 and k^s_h = 0.3, demonstrating strong foundation robustness. Conversely, for an eccentricity e/B = 0.25 (**Figure 4g**), the loss remains limited to around 17%, indicating that lateral confinement effectively mitigates the combined influence of e/B and k^s_h.

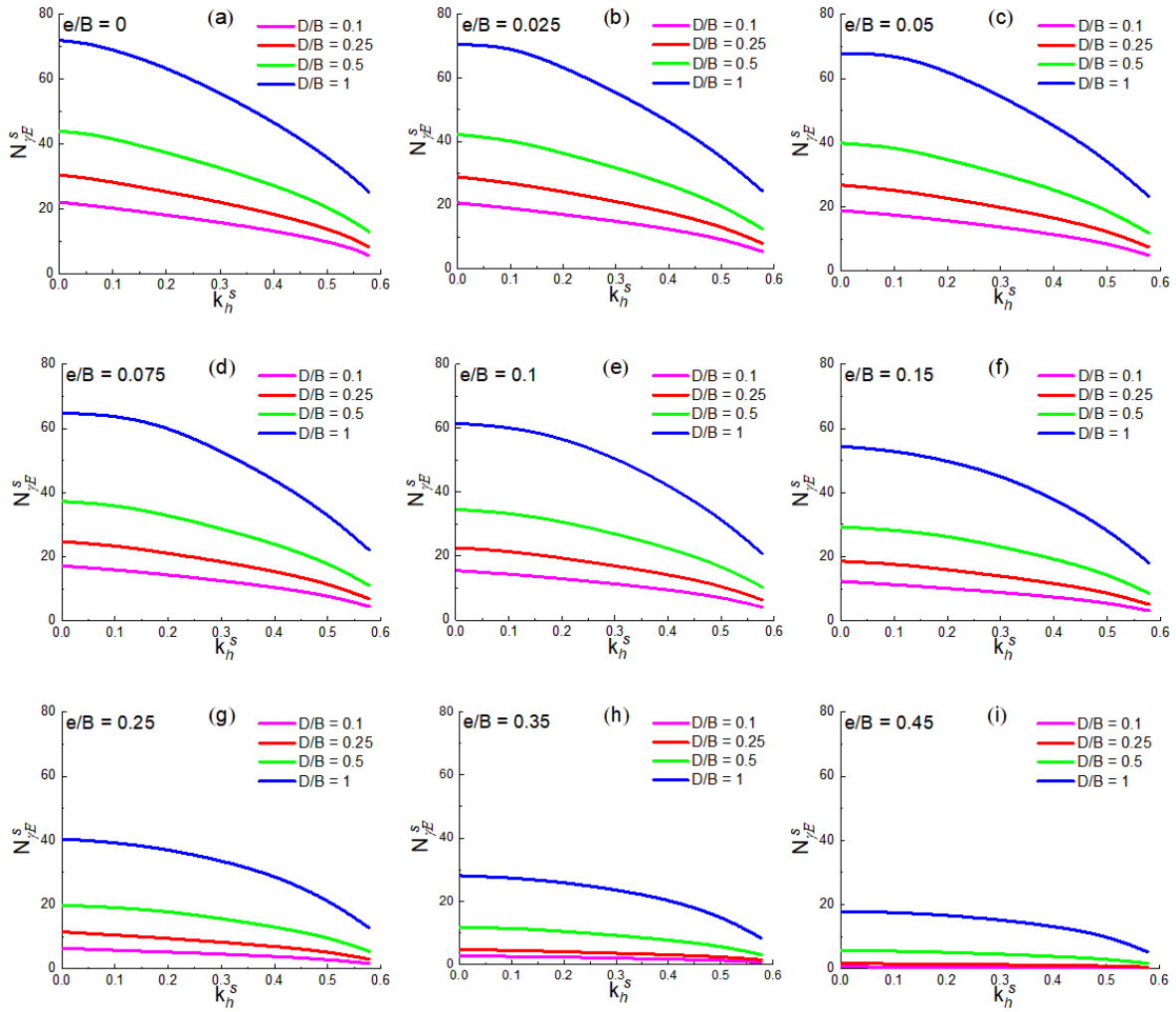

Figure 4. Seismic bearing capacity factor $N^s_{\gamma E}$ versus k^s_h due to soil inertia for different e/B and D/B ratios, with φ = 30°.

However, eccentricity remains a highly penalizing factor: at k_h^s = 0, the bearing capacity of a foundation with D/B = 1 decreases by approximately 44% when e/B increases from 0 to 0.25, whereas for a shallow skirt (D/B = 0.1), the reduction reaches nearly 70%. The beneficial effect of embedment becomes dominant: at k_h^s = 0.2, the capacity for D/B = 1 is roughly 3.5 times higher than that for D/B = 0.1 at e/B = 0, and nearly seven times higher at e/B = 0.25. The order of the curves remains consistent, the curvature becomes more pronounced at higher k_h^s values, and the relative efficiency of skirts increases with eccentricity—highlighting that a minimum embedment ratio $D/B \geq 0.5$ is recommended once $e/B \gtrsim 0.1$ and k_h^s approaches moderate levels (≈ 0.2–0.3).

Table 2 summarizes the evolution of the correction coefficient $e_{\gamma E}^s$ associated with soil inertia as a function of D/B, k_h^s, and e/B. Increasing k_h^s systematically reduces the coefficient value, reflecting the progressive degradation of bearing capacity under the growing influence of horizontal inertial forces. In contrast, increasing D/B significantly enhances foundation stability, confirming the beneficial role of skirts in mobilizing a larger soil mass and delaying failure initiation. Load eccentricity further reduces the coefficients, with this trend becoming more pronounced under higher seismic intensities. These findings underscore the necessity of simultaneously accounting for D/B, k_h^s, and e/B when assessing seismic bearing capacity, and they confirm the capability of the FELA model to accurately capture such complex interactions.

Table 2. Correction factor $e_{\gamma E}^s$ associated with soil inertia for different e/B, D/B ratios, and k_h^s values, with φ = 30°.

e/B		D/B			
	k_h	0.1	0.25	0.5	1
0	0	1.510	2.085	3.001	4.919
	0.1	1.384	1.929	2.846	4.719
	0.2	1.241	1.729	2.553	4.329
	0.3	1.082	1.509	2.229	3.807
	0.4	0.903	1.259	1.861	3.191
	0.5	0.681	0.951	1.405	2.454
	$tan\varphi$	0.389	0.568	0.890	1.727
0.025	0	1.406	1.970	2.881	4.810
	0.1	1.298	1.840	2.765	4.776
	0.2	1.163	1.650	2.481	4.331
	0.3	1.016	1.442	2.167	3.790
	0.4	0.849	1.205	1.810	3.173
	0.5	0.643	0.913	1.367	2.424
	$tan\varphi$	0.367	0.544	0.857	1.670
0.075	0.1	1.199	1.730	2.647	4.620
	0.2	1.075	1.553	2.376	4.260
	0.3	0.940	1.358	2.077	3.725
	0.4	0.787	1.137	1.736	3.109
	0.5	0.597	0.863	1.311	2.360
	$tan\varphi$	0.341	0.512	0.813	1.595
0.1	0	1.175	1.690	2.546	4.426
	0.1	1.094	1.608	2.478	4.382
	0.2	0.982	1.444	2.249	4.131
	0.3	0.859	1.264	1.968	3.613
	0.4	0.720	1.059	1.646	3.014
	0.5	0.547	0.805	1.244	2.277
	$tan\varphi$	0.312	0.475	0.762	1.514
	0	1.062	1.547	2.365	4.199
	0.1	0.987	1.479	2.293	4.131
	0.2	0.887	1.329	2.109	3.892
	0.3	0.776	1.164	1.845	3.469
	0.4	0.651	0.976	1.545	2.894
	0.5	0.496	0.743	1.168	2.180
	$tan\varphi$	0.282	0.436	0.707	1.428

Table 2. *Cont.*

e/B		D/B			
	k_h	**0.1**	**0.25**	**0.5**	**1**
0.15	0	0.848	1.273	2.004	3.718
	0.1	0.775	1.217	1.941	3.628
	0.2	0.697	1.094	1.811	3.414
	0.3	0.611	0.959	1.584	3.100
	0.4	0.514	0.805	1.326	2.607
	0.5	0.393	0.614	1.003	1.956
	tanφ	0.222	0.356	0.594	1.245
0.25	0	0.438	0.788	1.351	2.762
	0.1	0.400	0.721	1.310	2.693
	0.2	0.360	0.649	1.224	2.538
	0.3	0.316	0.570	1.070	2.306
	0.4	0.266	0.480	0.896	1.987
	0.5	0.205	0.368	0.676	1.478
	tanφ	0.115	0.206	0.379	0.877
0.35	0	0.189	0.329	0.808	1.920
	0.1	0.173	0.304	0.787	1.880
	0.2	0.156	0.276	0.719	1.776
	0.3	0.137	0.245	0.630	1.618
	0.4	0.116	0.211	0.529	1.402
	0.5	0.089	0.168	0.402	1.051
	tanφ	0.049	0.098	0.214	0.572
0.45	0	0.048	0.117	0.393	1.225
	0.1	0.044	0.109	0.382	1.204
	0.2	0.041	0.100	0.354	1.143
	0.3	0.037	0.090	0.314	1.045
	0.4	0.032	0.079	0.270	0.909
	0.5	0.026	0.065	0.214	0.714
	tanφ	0.016	0.042	0.117	0.361

Figure 5 presents the three-dimensional surfaces illustrating the variation of the correction coefficient $e^s_{\gamma E}$ as a function of e/B and k^s_h for different relative embedment depths D/B. These surfaces provide a clear 3D visualization of the combined influence of dynamic and geometric parameters on the corrected seismic bearing capacity. For shallow skirts (D/B = 0.1), the surface drops sharply when k^s_h > 0.2 and $e/B \geq 0.25$, indicating a strong sensitivity to the combined loading effects. Conversely, for deeper skirts (D/B = 1), the surfaces become significantly smoother, exhibiting gradual variations in $e^s_{\gamma E}$, confirming the role of lateral confinement in delaying failure and maintaining stable behavior.

From a practical perspective, these surfaces serve as a powerful interpretation and design tool, allowing engineers to visually identify safety zones ($e^s_{\gamma E}$ > 3) and delineate critical configurations likely to induce premature instability. They thus offer a robust basis for the development of design charts and the calibration of simplified analytical models for seismic design of skirted foundations.

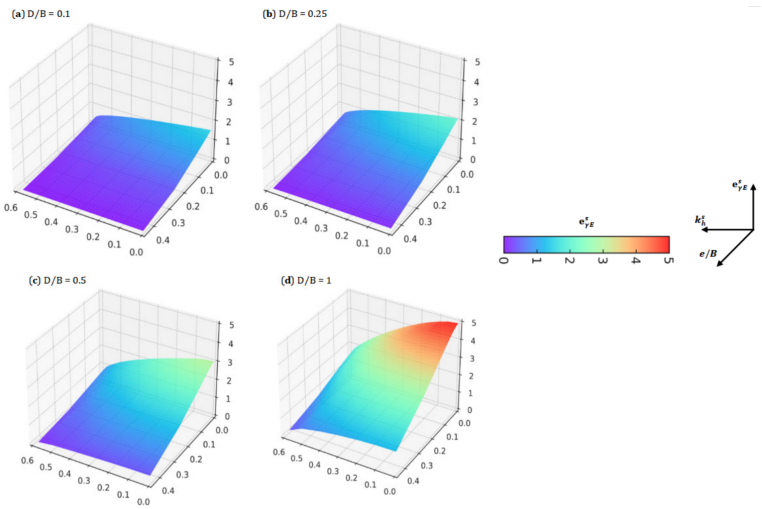

Figure 5. 3D surfaces of the correction factor $e^s_{\gamma E}$ associated with soil inertia for different e/B, D/B ratios, and k^s_h values, with φ = 30°.

Figure 6 illustrates the design curves of the seismic factor $N_{\gamma E}^{ss}$, which now incorporate the effect of superstructure inertia, for different relative skirt depths (D/B) and various eccentricity ratios (e/B). The results show a consistent decrease in $N_{\gamma E}^{ss}$ with increasing horizontal seismic coefficient k_h^{ss}, confirming the penalizing influence of superstructure inertia. This reduction is more pronounced for skirted shallow foundations, reflecting the limited mobilization of lateral resistance. For D/B = 0.1, the bearing capacity decreases rapidly as soon as k_h^{ss} > 0.2, particularly when e/B ≥ 0.25. In contrast, deep skirts (D/B = 1) ensure greater stability, with $N_{\gamma E}^{ss}$ values decreasing more gradually and remaining significantly higher under identical conditions. Eccentricity amplifies the loss of bearing capacity, especially when the superstructure transmits high overturning moments. These results confirm that the combination of large eccentricity and strong seismic excitation represents a critical scenario, whereas increasing D/B remains an effective reinforcement strategy.

Table 3 summarizes the evolution of the correction coefficient $e_{\gamma E}^{ss}$ as a function of D/B, k_h^{ss}, and e/B. Three main trends emerge: (i) an increase with D/B, confirming the stabilizing effect of skirts; (ii) a decrease with k_h^{ss}, illustrating the penalizing effect of superstructure inertia; and (iii) a reduction with e/B, since load eccentricity weakens bearing capacity even in the absence of seismic loading. The interaction between these parameters is particularly pronounced: for e/B = 0.25 and k_h^{ss} = 0.4, the value of $e_{\gamma E}^{ss}$ for D/B = 1 is nearly eleven times higher than that obtained for D/B = 0.1, emphasizing the efficiency of deep skirts in mitigating bearing capacity loss. These findings provide a direct basis for constructing three-dimensional design charts in the (D/B, k_h^{ss}, e/B) space.

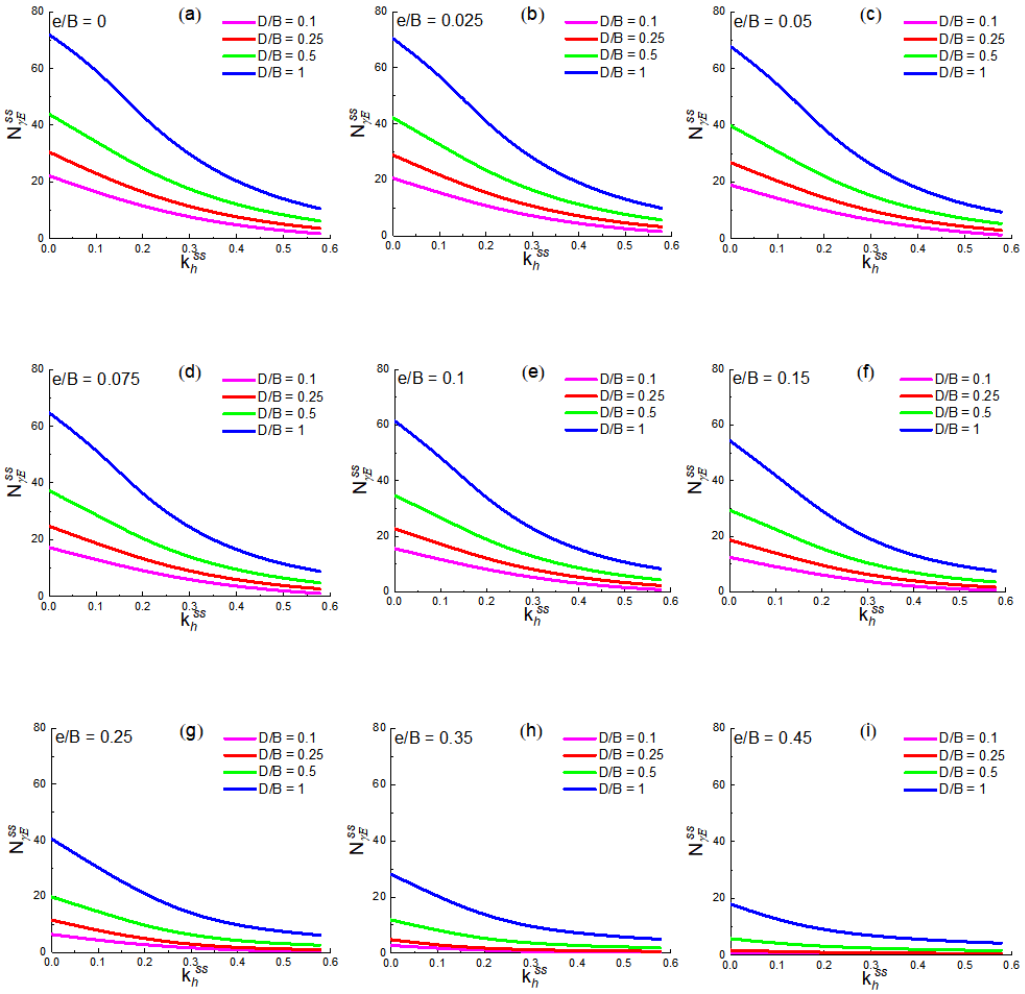

Figure 6. Seismic bearing capacity factor $N_{\gamma E}^{ss}$ versus k_h^{ss} due to superstructure inertia for different e/B and D/B ratios, with φ = 30°.

Table 3. Correction factor $e_{\gamma E}^{ss}$ associated with superstructure inertia for different e/B, D/B ratios, and k_h^{ss} values, with φ = 30°.

e/B		D/B			
	k_h	**0.1**	**0.25**	**0.5**	**1**
0	0	1.510	2.085	3.001	4.918
	0.1	1.116	1.560	2.334	4.113
	0.2	0.776	1.107	1.674	2.901
	0.3	0.512	0.761	1.171	1.985
	0.4	0.321	0.511	0.809	1.353
	0.5	0.189	0.338	0.560	0.938
	$tan\varphi$	0.119	0.245	0.424	0.722
0.025	0	1.406	1.970	2.881	4.810
	0.1	1.046	1.477	2.226	3.950
	0.2	0.727	1.042	1.578	2.744
	0.3	0.478	0.712	1.093	1.861
	0.4	0.296	0.474	0.750	1.263
	0.5	0.171	0.311	0.516	0.876
	$tan\varphi$	0.104	0.224	0.390	0.678
0.05	0	1.291	1.833	2.721	4.633
	0.1	0.967	1.382	2.101	3.765
	0.2	0.671	0.969	1.474	2.583
	0.3	0.438	0.657	1.013	1.739
	0.4	0.268	0.434	0.690	1.177
	0.5	0.150	0.282	0.472	0.817
	$tan\varphi$	0.085	0.202	0.356	0.638
0.075	0	1.175	1.690	2.546	4.426
	0.1	0.881	1.278	1.966	3.559
	0.2	0.609	0.891	1.367	2.422
	0.3	0.395	0.599	0.931	1.621
	0.4	0.237	0.392	0.630	1.094
	0.5	0.126	0.252	0.429	0.762
	$tan\varphi$	0.067	0.178	0.324	0.602
0.1	0	1.062	1.547	2.365	4.199
	0.1	0.792	1.169	1.825	3.323
	0.2	0.544	0.809	1.258	2.263
	0.3	0.348	0.539	0.850	1.505
	0.4	0.203	0.349	0.571	1.016
	0.5	0.100	0.222	0.388	0.712
	$tan\varphi$	0.054	0.155	0.293	0.569
0.15	0	0.848	1.273	2.004	3.718
	0.1	0.612	0.947	1.538	2.871
	0.2	0.409	0.643	1.040	1.955
	0.3	0.248	0.418	0.691	1.289
	0.4	0.131	0.262	0.459	0.872
	0.5	0.064	0.161	0.312	0.626
	$tan\varphi$	0.038	0.113	0.243	0.512
0.25	0	0.438	0.788	1.351	2.762
	0.1	0.294	0.526	0.992	2.057
	0.2	0.182	0.328	0.642	1.404
	0.3	0.106	0.191	0.416	0.926
	0.4	0.058	0.114	0.280	0.651
	0.5	0.032	0.081	0.209	0.497
	$tan\varphi$	0.022	0.066	0.174	0.419
0.35	0	0.189	0.329	0.808	1.920
	0.1	0.121	0.194	0.551	1.371
	0.2	0.072	0.119	0.346	0.913
	0.3	0.042	0.083	0.242	0.636
	0.4	0.025	0.064	0.186	0.485
	0.5	0.017	0.052	0.151	0.392
	$tan\varphi$	0.014	0.045	0.132	0.340
0.45	0	0.048	0.117	0.393	1.225
	0.1	0.031	0.082	0.278	0.841
	0.2	0.020	0.063	0.207	0.598
	0.3	0.015	0.051	0.164	0.462
	0.4	0.012	0.043	0.136	0.377
	0.5	0.010	0.037	0.117	0.318
	$tan\varphi$	0.008	0.033	0.105	0.283

Finally, **Figure 7** presents the three-dimensional surfaces of the coefficient $e_{\gamma E}^{ss}$, expressed as a function of k_h^{ss} and e/B for several relative depths D/B. The resulting surfaces clearly illustrate the mechanisms of bearing capacity degradation under inertial effects. For shallow skirts, the surface slope is steeper, and $e_{\gamma E}^{ss}$ decreases rapidly once k_h^{ss} > 0.2, especially when $e/B \geq 0.2$. Conversely, deep skirted foundations ($D/B \approx 0.75$–1.0) exhibit much more stable surfaces, indicating a better redistribution of stresses due to increased passive soil resistance. Unlike soil inertia, which acts locally within the failure zone, superstructure inertia acts globally at the foundation base, giving these results special significance for massive structures such as offshore platforms, storage tanks, and tall towers. These graphical representations enable the identification of critical zones, safe configurations ($e_{\gamma E}^{ss}$ > 3), and performance thresholds necessary to ensure seismic stability. They also represent a powerful design tool, forming a solid basis for developing generalized equations and simplified design guidelines adapted to complex dynamic loading conditions.

It should be emphasized that the seismic bearing capacity factors remain dependent on the soil mechanical properties and soil–foundation interface conditions. Variations in the friction angle φ, interface roughness (δ/φ), or the presence of cohesion may significantly influence the failure mechanism and the variation of bearing capacity under seismic loading. Therefore, the present results and correction factors should be interpreted within the framework of the investigated assumptions corresponding to a homogeneous purely frictional soil with $\varphi = 30°$, $c = 0$, and a perfectly rough interface condition.

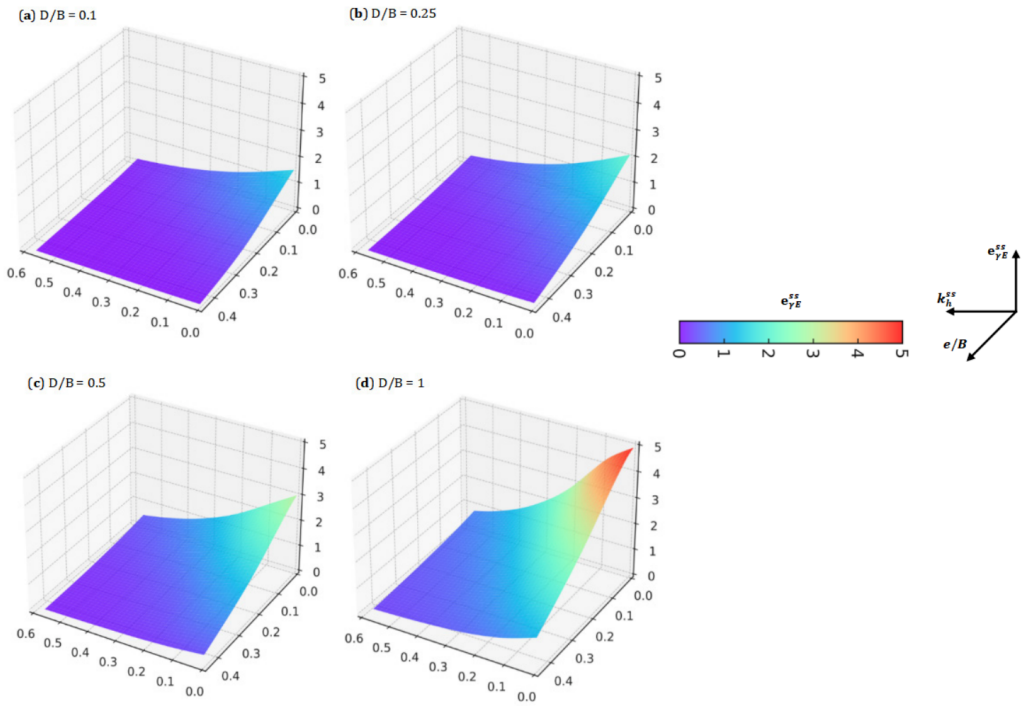

Figure 7. 3D surfaces of the correction factor $e_{\gamma E}^{ss}$ associated with superstructure inertia for different e/B, D/B ratios, and k_h^{ss} values, with φ = 30°.

3.1. Proposed Design Equations

The formulation of simple and generalizable analytical equations represents a major step toward translating numerical findings into practical geotechnical design applications. Although Finite Element Limit Analysis (FELA) simulations are highly accurate, they remain computationally demanding for routine engineering use. Therefore, there is a need for reliable correction equations that simultaneously account for the effects of eccentricity, embedment depth, and seismic loading. The proposed relationships meet this objective by providing a compact analytical form that effectively captures the key behavioral trends derived from the full set of para-

metric analyses.

Deriving generalized analytical correction factors from numerical simulations provides an efficient way to transform advanced FELA results into practical engineering design tools. In this study, the proposed equations were developed from an extensive numerical database in order to capture the combined effects of seismic loading, embedment depth, and load eccentricity within a simplified analytical framework[4, 34].

To quantify the combined influence of load eccentricity, relative skirt depth, and horizontal seismic coefficient on the bearing capacity associated with soil inertia, a generalized equation for the seismic correction factor $e^s_{\gamma E}$ has been developed. The adopted formulation is based on a nonlinear allometric-type law capable of accurately reproducing the interactions among geometric and dynamic parameters:

$$e^s_\gamma = \left[a_1 \bullet \frac{D}{B} + a_2\right] + \left[\left(a_3 \bullet \frac{D}{B} + a_4\right) \bullet k_h^{s\,a_5}\right] \quad (3)$$

where the coefficients a_1 through a_5 are expressed as second-order polynomial functions of the eccentricity ratio e/B:

$$a_i = \alpha_i (e/B)^2 + \beta_i (e/B) + \gamma_i \quad (4)$$

The numerical parameters α, β, and γ are provided in **Table 4**, allowing direct implementation of the model within the investigated domain. This compact expression effectively captures the coupled effects of the three primary variables while remaining suitable for design-stage application.

Table 4. Coefficients a_i and parameters α, β, and γ for the proposed analytical equation associated with soil inertia.

	α	β	γ
a_1	−2.870	−4.869	4.052
a_2	8.516	−5.788	1.050
a_3	42.003	−16.771	−5.786
a_4	−4.441	8.305	−1.975
a_5	−1.419	2.369	1.646

A comparison between the predictions obtained from the proposed equation and the results from the FELA simulations demonstrates excellent agreement (**Figure 8**). The coefficient of determination reaches R^2 = 0.983, the root-mean-square error remains low (*RMS* = 0.159), and both the arithmetic mean (*Mean* = 1.549) and coefficient of variation (*Cov* = 1.463) confirm the correlation's stability. These results validate the robustness and reliability of the proposed model, which faithfully reproduces the numerical trends while being easily integrable into seismic bearing-capacity design procedures for skirted foundations. Furthermore, the relatively low *RMS* value and the limited dispersion of the data around the equality line indicate that the deviations between the analytical predictions and the FELA results remain small over the entire investigated parameter range. The proposed formulation therefore provides a consistent approximation of the numerical solutions and accurately captures the progressive reduction in seismic bearing capacity associated with increasing soil inertia effects.

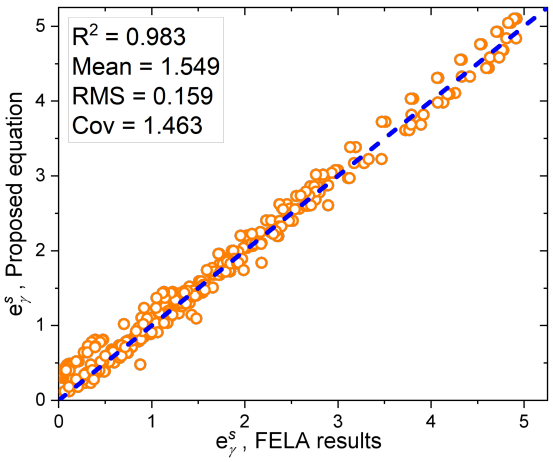

Figure 8. Performance of the proposed analytical Equation (3) compared with FELA solutions associated with soil inertia.

For the superstructure inertia, a second generalized equation was formulated based on the FELA results covering a wide range of parameters (e/B, D/B, k_h^{ss}). This equation features an asymptotic nonlinear structure combining exponential and polynomial terms, reflecting the complexity of the soil–foundation–

superstructure interaction mechanisms:

$$e_{\gamma}^{ss} = \left[a_1 \bullet e^{a_2 \bullet \frac{D}{B}}\right] - \left[\left(a_3 + a_4 \bullet \frac{D}{B}\right) a_5{}^{k_h^{ss}}\right] \quad (5)$$

where the coefficients a_1 to a_5 are expressed as cubic polynomial functions of the eccentricity ratio e/B:

$$a_i = \alpha_i (e/B)^3 + \beta_i (e/B)^2 + \gamma_i (e/B) + \delta_i, \quad i = 1, \ldots 5 \quad (6)$$

The corresponding numerical coefficients α, β, γ, and δ are listed in **Table 5**, allowing direct implementation of the model for any value of e/B within the studied range.

The validation of this formulation, by comparison with FELA results, demonstrates an exceptionally high level of correlation (**Figure 9**). The coefficient of determination reaches R^2 = 0.988, the root mean square error remains very low (*RMS* = 0.108), the arithmetic mean is close to unity (*Mean* = 0.946), and the coefficient of variation (*Cov* = 1.042) indicates minimal dispersion around the equality line. These statistical performances confirm the generality and reliability of the proposed equation for the practical assessment of the superstructure inertia effect in the seismic bearing capacity analysis of shallow foundations. In addition, the very low *RMS* value and the limited scatter of the results around the equality line demonstrate that the analytical predictions remain very close to the numerical FELA solutions throughout the investigated parameter range. The proposed formulation successfully reproduces the nonlinear evolution of the seismic correction factor and accurately captures the progressive destabilizing influence induced by increasing superstructure inertia.

Table 5. Coefficients a_i and parameters α, β, γ and δ for the proposed analytical equation associated with superstructure inertia.

	α	β	γ	δ
a_1	−20.341	13.448	−1.526	−0.175
a_2	401.271	−174.255	1.299	1.719
a_3	−40.895	23.632	0.463	−1.117
a_4	34.062	−29.413	15.235	−5.102
a_5	2.596	−1.451	−0.036	0.082

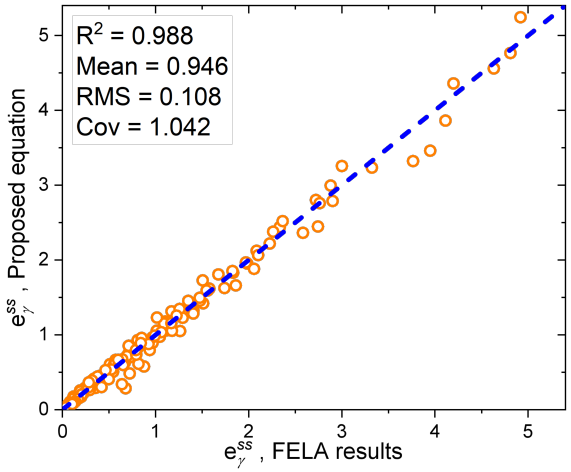

Figure 9. Performance of the proposed analytical Equation (5) compared with FELA solutions associated with superstructure inertia.

Hence, the two proposed formulations together provide a rigorous and operational analytical framework for evaluating coupled inertial effects. They constitute a solid foundation for developing design charts, calibrating empirical relationships, and establishing simplified design methods adapted to massive structures and complex seismic environments.

Although the proposed equations were calibrated and validated using the numerical database generated in the present FELA study, they provide a consistent predictive framework within the investigated parameter range, namely $\varphi = 30°$, $k_v = 0$, $0 \leq k_h \leq \tan\varphi$, $0.1 \leq D/B \leq 1$, and $0 \leq e/B \leq 0.45$, assuming a perfectly rough base–skirt–soil interface $(\delta/\varphi = 1)$. It should be noted that independent validation using experimental observations, centrifuge tests, or published seismic data specifically addressing the separate effects of soil and superstructure inertia on offshore skirted foundations remains limited in the current literature. Therefore, future research should focus on extending the validation of the proposed formulations through additional experimental and numerical investigations in order to further enhance their scientific reliability and practical applicability.

3.2. Failure Mechanisms

To complement the quantitative evaluation of seismic bearing capacity, the failure mechanisms obtained from the FELA simulations are analyzed to provide a mechanical interpretation of the observed trends, focusing on the development of plastic zones, the mobilization of soil resistance, and the evolution of failure patterns under eccentric and seismic loading. The analysis is carried out for representative cases defined by two eccentricity ratios (e/B = 0 and 0.2), a fixed embedment ratio (D/B = 0.5), and three values of the horizontal seismic coefficient (k_h = 0, 0.1, and 0.25). This framework enables a consistent comparison of failure mechanisms under increasing seismic intensity, while highlighting the distinct roles of soil inertia and superstructure inertia, which are discussed separately.

Figure 10 illustrates the failure mechanisms associated with soil inertia. For $k_h^s = 0$, the centered case shows a nearly symmetric and confined mechanism beneath the foundation, reflecting the stabilizing role of skirt embedment. When eccentricity is introduced $(e/B = 0.2)$, the mechanism becomes asymmetric, with plastic deformation concentrated beneath the loaded side. As k_h^s increases, the failure pattern progressively shifts and becomes more inclined in the direction of seismic inertia, with lateral extension of the plastic zone. At $k_h^s = 0.25$, a well-defined inclined shear band develops from the skirt tip toward the ground surface. In the eccentric case, the combined effect of inertia and load eccentricity enhances deformation localization and promotes a rotational tendency. Overall, skirt embedment increases confinement and delays failure, although increasing k_h^s and e/B progressively reduces stability and leads to asymmetric mechanisms.

In addition, the increase in seismic intensity leads to a progressive redistribution of stresses and a deeper propagation of the plastic zones beneath the foundation. The inclined shear bands become more pronounced as k_h^s increases, indicating a transition from a relatively confined bearing mechanism toward a coupled sliding–rotation mode. For the eccentric configurations, deformation localization becomes significantly concentrated beneath the heavily loaded side, while the mobilized soil volume decreases on the opposite side. These observations confirm that increasing seismic inertia not only enlarges the extent of plasticization but also accelerates the instability of the foundation system through progressive asymmetry and stress concentration.

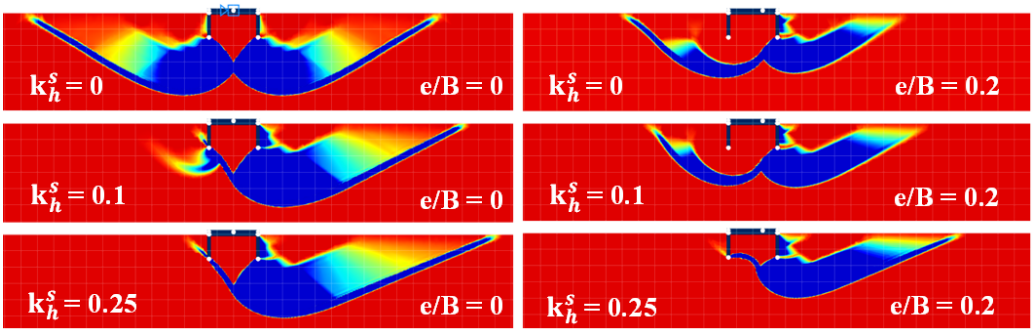

Figure 10. Failure mechanisms induced by soil inertia.

Figure 11 presents the failure mechanisms associated with superstructure inertia. For $k_h^{ss} = 0$, the centered case exhibits a symmetric confined mechanism similar to static conditions, while eccentricity induces an asymmetric distribution of plastic strains. As k_h^{ss} increases, the failure mechanism evolves more rapidly than in the soil inertia case, with a pronounced inclination of the shear band and a progressive shift of the plastic zone. This behavior reflects the global action of superstructure inertia, which generates additional shear and overturning effects at the foundation level. At $k_h^{ss} = 0.25$, the mechanism becomes strongly asymmetric, with a reduced effective bearing zone and a dominant rotational mode in the eccentric case.

Furthermore, the increase in k_h^{ss} intensifies stress redistribution beneath the foundation and promotes a

progressive localization of deformation near the loaded edge. Compared with the soil inertia case, the plastic zones become more concentrated and the rotational component of the mechanism develops more rapidly, indicating a stronger destabilizing effect associated with overturning moments transmitted by the superstructure. The progressive reduction of the effective bearing area and the extension of inclined shear bands toward the ground surface clearly illustrate the transition from a confined bearing mechanism to a predominantly rotation-controlled failure mode under high seismic intensity.

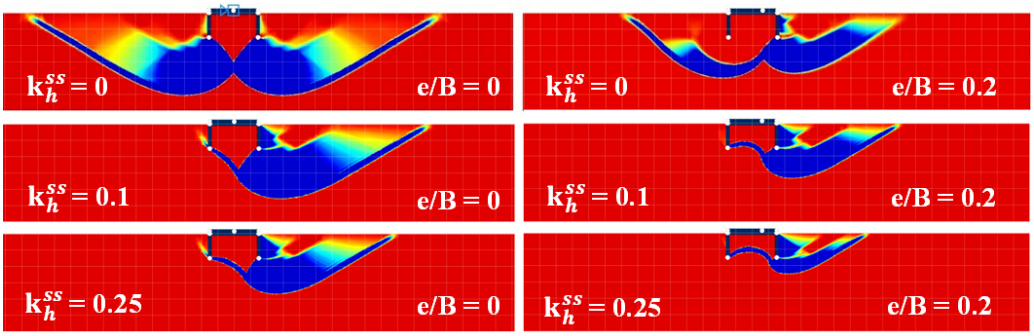

Figure 11. Failure mechanisms induced by superstructure inertia.

Overall, the comparison between **Figures 10** and **11** highlights a fundamental difference between the two inertial effects: soil inertia mainly influences the local development of plastic zones within the failure region, whereas superstructure inertia induces a more global destabilization mechanism governed by overturning and base shear. These findings provide a clearer mechanical interpretation of the bearing capacity reduction observed in the parametric study.

4. Limitations of the Study

The present study is based on a pseudo-static approach, in which the seismic action is modeled by a constant horizontal acceleration coefficient (k_h), while the vertical acceleration is neglected (k_v = 0). This simplification does not allow for the reproduction of transient effects, cyclic loading conditions, or the actual propagation of seismic waves, which may influence the evolution of failure mechanisms and the mobilization of soil resistance. The mechanical properties of the soil are assumed to remain constant during shaking, without modeling degradation, cyclic dilatancy, soil softening, or liquefaction phenomena, which could lead to a further reduction in bearing capacity under real seismic conditions.

The analysis was carried out for a single friction angle (φ = 30°), representative of medium-density sand, without accounting for the variability of soil properties or stratification. In addition, the inertial effects of the soil and the superstructure were studied separately, without considering their combined interaction, which limits the generalization of the results to cases involving simultaneous excitation.

Finally, the modeling was restricted to purely frictional soils (c = 0) and rigid skirted foundations analyzed under plane-strain (2D) conditions. While this assumption enables an efficient representation of the failure mechanisms, it does not capture three-dimensional effects, which may influence stress redistribution and failure geometry in real foundations. Although these assumptions are commonly adopted for an initial parametric investigation, they provide a consistent basis for future studies incorporating three-dimensional response, soil variability, cyclic loading, and fully dynamic analyses, in order to better represent the real seismic behavior of skirted foundations.

Future research perspectives include extending the proposed framework to different friction angles, partially rough interfaces, combined effects, and more complex seismic loading conditions involving both horizontal and vertical accelerations. Additional investigations considering c - φ soils, layered deposits, cyclic degradation, and liquefaction effects would further improve the applicability of the proposed equations. Moreover, the

extension toward fully coupled dynamic analyses and three-dimensional foundation geometries represents an important step toward a more realistic assessment of the seismic behavior of offshore skirted foundations under practical field conditions.

5. Conclusions

This study analyzed the seismic bearing capacity of skirted foundations subjected to an eccentric vertical load, distinguishing between the effects of soil inertia and superstructure inertia using Finite Element Limit Analysis (FELA) with the OptumG2 software, with explicit separation of soil and superstructure inertia. The main findings can be summarized as follows:

- Increasing the embedment ratio (D/B) significantly improves stability, whereas both load eccentricity (e/B) and the horizontal seismic coefficient (k_h) lead to a progressive reduction in bearing capacity. Deep skirts effectively mitigate these effects, confirming their stabilizing role.
- Both soil inertia and superstructure inertia exert a detrimental influence, more pronounced in shallow or highly eccentric configurations. Superstructure inertia acts globally on overall stability, while soil inertia affects the local bearing zone beneath the foundation.
- Two generalized equations were proposed for the correction factors $e^{s}_{\gamma E}$ and $e^{ss}_{\gamma E}$, accurately reproducing the numerical results with $R^2 > 0.98$. These models provide a reliable and practical tool for rapidly estimating the corrected seismic bearing capacity of skirted foundations.

In practice, the results provide useful thresholds for the seismic design of skirted foundations. A minimum embedment ratio of $D/B \geq 0.5$ is recommended to ensure sufficient confinement, while an eccentricity ratio exceeding $e/B \approx 0.1$ significantly reduces bearing capacity. The horizontal seismic coefficient should preferably remain below $k_h \approx 0.2$–0.25, particularly for shallow foundations ($D/B \leq 0.1$), which should be avoided in seismic regions. These findings offer practical guidance for design and assessment.

Author Contributions

Conceptualization, A.B. and N.Z.; methodology, A.B. and N.Z.; software, A.B.; validation, A.B. and N.Z.; formal analysis, A.B.; investigation, A.B.; data curation, A.B.; writing—original draft preparation, A.B.; writing—review and editing, A.B. and N.Z.; visualization, A.B.; supervision, N.Z. Both authors have read and agreed to the published version of the manuscript.

Funding

This work was supported by the Directorate General for Scientific Research and Technological Development (DGRSDT) and the Ministry of Higher Education and Scientific Research (MESRS, Algeria), which provided financial support and research facilities.

Institutional Review Board Statement

Not applicable.

Informed Consent Statement

Not applicable.

Data Availability Statement

The numerical data supporting the findings of this study are available from the corresponding author upon reasonable request. All simulations were performed using licensed software; input and output files are available upon request for academic use.

Acknowledgments

The authors would like to express their sincere gratitude to the Directorate General for Scientific Research and Technological Development (DGRSDT) and the Ministry of Higher Education and Scientific Research (MESRS, Algeria) for their financial support. The authors also acknowledge the Scientific and Technical Research Center on Arid Regions (CRSTRA) for providing the necessary research facilities.

Conflicts of Interest

The authors declare no conflict of interest.

AI Use Statement

During the preparation of this manuscript, the authors used generative artificial intelligence tools, such as Grammarly, QuillBot, and ChatGPT, solely for language refinement and text editing. No AI tools were used for data analysis, interpretation, or generation of scientific content. All outputs were critically reviewed and validated by the authors, and the authors take full responsibility for the integrity and accuracy of the work.

References

[1] Terzaghi, K., 1943. Theoretical Soil Mechanics. John Wiley & Sons: New York, NY, USA.

[2] Frydman, S., Burd, H.J., 1997. Numerical Studies of Bearing Capacity Factor Nγ. Journal of Geotechnical and Geoenvironmental Engineering. 123(1), 20–29. DOI: https://doi.org/10.1061/(ASCE)1090-0241(1997)123:1(20)

[3] Loukidis, D., Chakraborty, T., Salgado, R., 2008. Bearing Capacity of Strip Footings on Purely Frictional Soil under Eccentric and Inclined Loads. Canadian Geotechnical Journal. 45(6), 768–787. DOI: https://doi.org/10.1139/T08-015

[4] Bouaicha, A., Mabrouki, A., 2024. Failure Envelopes for Strip Footings on Sand Overlying Non-Homogeneous Clay under Combined Loading. Transportation Infrastructure Geotechnology. 11, 44–62. DOI: https://doi.org/10.1007/s40515-022-00272-0

[5] Bransby, M.F., Randolph, M.F., 1998. Combined Loading of Skirted Foundations. Géotechnique. 48(5), 637–655. DOI: https://doi.org/10.1680/geot.1998.48.5.637

[6] Hu, Y., Randolph, M.F., Watson, P.G., 1999. Bearing Response of Skirted Foundation on Non-Homogeneous Soil. Journal of Geotechnical and Geoenvironmental Engineering. 125(11), 924–935. DOI: https://doi.org/10.1061/(ASCE)1090-0241(1999)125:11(924)

[7] Yun, G., Bransby, M.F., 2007. The Undrained Vertical Bearing Capacity of Skirted Foundations. Soils and Foundations. 47(3), 493–505. DOI: https://doi.org/10.3208/sandf.47.493

[8] Selmi, M., Kormi, T., Hentati, A., et al., 2019. Capacity Assessment of Offshore Skirted Foundations under HM Combined Loading Using RFEM. Computers and Geotechnics. 114, 103148. DOI: https://doi.org/10.1016/j.compgeo.2019.103148

[9] Mana, D., Gourvenec, S., Randolph, M., 2010. A Numerical Study of the Vertical Bearing Capacity of Skirted Foundations. In Frontiers in Offshore Geotechnics II. CRC Press: Boca Raton, FL, USA. pp. 433–438.

[10] Eid, H.T., 2013. Bearing Capacity and Settlement of Skirted Shallow Foundations on Sand. International Journal of Geomechanics. 13(5), 645–652. DOI: https://doi.org/10.1061/(ASCE)GM.1943-5622.0000237

[11] Al-Aghbari, M.Y., Mohamedzein, Y.E.A., 2004. Model Testing of Strip Footings with Structural Skirts. Proceedings of the Institution of Civil Engineers - Ground Improvement. 8(4), 171–177. DOI: https://doi.org/10.1680/grim.8.4.171.41844

[12] Bouaicha, A., Boumekik, N.E.I., Mabrouki, A., 2025. Numerical Investigation of the Seismic Bearing Capacity of Offshore Skirted Foundations Installed in Sand Using Finite Element Limit Analysis. Materials Research Proceedings. 48, 161–170. DOI: https://doi.org/10.21741/9781644903414-19

[13] Sarma, S.K., Iossifelis, I.S., 1990. Seismic Bearing Capacity Factors of Shallow Strip Footings. Géotechnique. 40(2), 265–273. DOI: https://doi.org/10.1680/geot.1990.40.2.265

[14] Richards, R., Elms, D.G., Budhu, M., 1993. Seismic Bearing Capacity and Settlement of Foundations. Journal of Geotechnical Engineering. 119(4), 662–674. DOI: https://doi.org/10.1061/(ASCE)0733-9410(1993)119:4(662)

[15] Paolucci, R., Pecker, A., 1997. Seismic Bearing Capacity of Shallow Strip Foundations on Dry Soils. Soils and Foundations. 37(3), 95–105. DOI: https://doi.org/10.3208/sandf.37.3_95

[16] Cascone, E., Casablanca, O., 2016. Static and Seismic Bearing Capacity of Shallow Strip Footings. Soil Dynamics and Earthquake Engineering. 84, 204–223. DOI: https://doi.org/10.1016/j.soildyn.2016.02.010

[17] Chamekh, A., Bouaicha, A., Messai, A., 2025. Effects of Soil and Superstructure Inertia on the Seismic Bearing Capacity of Shallow Foundations under Eccentric Loading Using Finite Element Limit Analysis. Transportation Infrastructure Geotechnology. 12, 234. DOI: https://doi.org/10.1007/s40515-025-00692-8

[18] Pal, A., Ghosh, P., Majumder, M., 2017. Interaction Effect of Two Closely Spaced Skirted Strip Foundations in Cohesionless Soil Using Upper-Bound Limit Analysis. International Journal of Geomechanics. 17(2). DOI: https://doi.org/10.1061/(ASCE)GM.1943-5622.0000755

[19] Ghosh, P., Pal, A., 2019. Undrained Bearing Capac-

ity of a Skirted Foundation Using Upper-Bound Limit Analysis. Acta Geotechnica Slovenica. 16(2), 2–11.

[20] Santhoshkumar, G., Ghosh, P., 2020. Ultimate Bearing Capacity of Skirted Foundation on Cohesionless Soil Using Slip Line Theory. Computers and Geotechnics. 123, 103573. DOI: https://doi.org/10.1016/j.compgeo.2020.103573

[21] Ding, H., Pan, C., Zhang, P., et al., 2022. Shaking Table Tests and Seismic Response of Three-Bucket Jacket Foundations for Offshore Wind Turbines. Journal of Ocean University of China. 21, 719–736. DOI: https://doi.org/10.1007/s11802-022-4742-7

[22] Beygi, M., Fallahi, M., Vali, R., et al., 2023. FELA-DNN Framework to Predict the Seismic Bearing Capacity of Skirted Strip Footing Built on a Non-Cohesive Slope. Soil Dynamics and Earthquake Engineering. 171, 107932. DOI: https://doi.org/10.1016/j.soildyn.2023.107932

[23] Chauhan, V.B., Singh, T., Verma, S., et al., 2025. Adaptive FELA and Machine Learning for Skirted Footing Performance under Inclined Loading. Transportation Infrastructure Geotechnology. 12, 293. DOI: https://doi.org/10.1007/s40515-025-00753-y

[24] Datta, N.V., Khuntia, S., 2026. Seismic Bearing Capacity Analysis of Skirted Footing on Cohesive-Frictional Soil Slopes. In: Bhandary, N.P., Tiwari, B., Acharya, I.P., et al. (eds.). Proceedings of GeoMandu 2024 Volume 1. Springer: Singapore. DOI: https://doi.org/10.1007/978-981-96-7921-8_17

[25] Verma, S., Datta, S., Chauhan, V.B., 2026. Seismic Bearing Capacity of Skirted Footings on Cohesive Slopes Using Limit Analysis. Proceedings of the Indian National Science Academy. DOI: https://doi.org/10.1007/s43538-026-00717-x

[26] Zhou, H., Liu, Z., Shao, J., et al., 2026. Effects of Stress Direction and Magnitude on Strength and Failure of Weakly Anisotropic Sandstone under True Triaxial Compression. Rock Mechanics and Rock Engineering. 59, 3213–3234. DOI: https://doi.org/10.1007/s00603-025-04982-y

[27] Optum Computational Engineering, 2023. OptumG2—2D Geotechnical Design & Analysis Software. Available from: https://optumce.com/optum-g2/ (cited 1 March 2026).

[28] Lai, V.Q., Shiau, J., Promwichai, T., et al., 2023. Modelling Soil Stability in Wide Tunnels Using FELA and Multivariate Adaptive Regression Splines Analysis. Modeling Earth Systems and Environment. 9, 2993–3008. DOI: https://doi.org/10.1007/s40808-022-01595-0

[29] Keawsawasvong, S., Kounlavong, K., Duong, N.T., et al., 2024. Seismic Stability Assessment of Rock Slopes Using Multivariate Adaptive Regression Splines. Transportation Infrastructure Geotechnology. 11, 2296–2318. DOI: https://doi.org/10.1007/s40515-024-00374-x

[30] Chen, X., Wang, Z., Kong, D., et al., 2025. Development of an Adaptive Meshing Upper Bound Limit Analysis Method for Large Deformation Axisymmetric Geotechnical Problems. Scientific Reports. 15, 5771. DOI: https://doi.org/10.1038/s41598-025-89033-w

[31] Tran, D.T., Shiau, J., Keawsawasvong, S., et al., 2025. Failure Envelopes of Embedded Foundations under V-H-M Loadings in Anisotropic Clays Using Optimised ANFIS Algorithms. Marine Georesources and Geotechnology. 43(10), 1900–1917. DOI: https://doi.org/10.1080/1064119X.2024.2440553

[32] Mohapatra, D., Kumar, J., 2020. Bearing Capacity of Embedded Foundations Using Quasi-Kinematic Limit Analysis. Computers and Geotechnics. 117, 103275. DOI: https://doi.org/10.1016/j.compgeo.2019.103275

[33] Conti, R., 2018. Simplified Formulas for the Seismic Bearing Capacity of Shallow Strip Foundations. Soil Dynamics and Earthquake Engineering. 104, 64–74. DOI: https://doi.org/10.1016/j.soildyn.2017.09.027

[34] Tian, Z., Liu, K., Malik, A., 2026. An Experimental Method for Turbine Rotors Based on Temperature Correction. Aerospace Science and Technology. 177, 112237. DOI: https://doi.org/10.1016/j.ast.2026.112237